

STRUCTURAL RELIABILITY OF HOLLOW CORE SLABS CONSIDERING COMPRESSIVE MEMBRANE ACTION

THOMAS THIENPONT*, RUBEN VAN COILE, WOUTER DE CORTE,
ROBBY CASPEELE

Ghent University, Department of Structural Engineering and Building Materials, Technologiepark-Zwijnaarde 60, 9052 Ghent, Belgium

* corresponding author: Thomas.Thienpont@ugent.be

ABSTRACT. Compressive membrane action can considerably improve the load bearing capacity of concrete slabs and beams in case of excessive loading due to an accidental event. Currently, only limited research has been focusing on compressive membrane action in prestressed concrete elements, or on concrete elements with large cavities, such as precast concrete hollow core slabs. Therefore, a novel real-scale test setup has been developed in order to assess this effect in precast hollow core slabs, and how it can enhance the load-carrying capacity in accidental events. In parallel with these tests, a numerical finite element model has been developed in order to perform a more detailed structural analysis of this phenomenon, and to study the influence of various input parameters. The details of this test setup are briefly explained, and some relevant experimental test results are provided. Considering the experimental findings and validated numerical model, this contribution aims to quantify the influence of compressive membrane action on the structural reliability of precast concrete hollow core slabs. To this end, probabilistic models for the most important material and geometric variables are gathered, and the structural reliability is assessed using Latin Hypercube sampling. Overall, the results indicate that considering the formation of compressive membrane action strongly influences the variability of the ultimate load-carrying capacity of precast concrete hollow core slabs.

KEYWORDS: Cost optimization, structural reliability, target reliability.

1. INTRODUCTION

When an axially restrained concrete slab is excessively loaded (e.g. due to an accidental event), compressive membrane action (CMA) can be activated, which can considerably enhance the load-carrying capacity. This can delay or even prevent a progressive collapse, increase the structural reliability and consequently increase the robustness of concrete structures. The general principle of CMA in an axially restrained slab is illustrated in Figure 1.

Although this effect was already investigated by other researches [1–4], most investigations focus on reinforced concrete members. So far, very little attention has been paid to the role of membrane action in prestressed concrete members. Furthermore, only limited research has been focusing on CMA in concrete members with large cavities, such as hollow core (HC) slabs. HC slabs are nowadays very commonly used, with the annual global production of these elements reaching 50 million m² [5], and a better understanding of how CMA could affect the behaviour of these slabs is needed. In a recent study, the beneficial effect of CMA on the load-carrying capacity of precast HC slabs has been demonstrated experimentally [6]. In parallel, a numerical finite element (FE) model was established in order to model the structural behaviour (i.e. compressive membrane action) as per the investigated test program.

In this contribution, the details of the experimental test setup and the numerical model are briefly discussed, and some relevant experimental test results are provided. Next, the numerical model is employed to perform a stochastic FE analysis of the ultimate load-carrying capacity. Herewith, this paper undertakes some first steps to quantify and incorporate the uncertainties which are associated to the development of compressive membrane action in precast HC slabs exposed to excessive loading.

2. NOVEL EXPERIMENTAL TEST SETUP

The beneficial effect of CMA on the load-carrying capacity of HC slabs was demonstrated in an experimental study by [6], as illustrated in Figure 2. Herein, three tests were performed: two axially restrained tests (labelled HC1 and HC2) and one unrestrained test (labelled HC3). The tests were carried out on HC slabs casted by a local Belgian producer, with a length of 10.4 m and a 1200 mm × 320 mm cross section (see Figure 3). In both the restrained and the unrestrained tests, the slabs were loaded in a four-point bending setup. The slabs were supported by two roller supports at a distance of 1 m from the slab end (resulting in a free span of 8.4m) and the loads were applied at 1/4th of the span length. In the restrained tests, the horizontal outward displacements of the HC slab were restrained by four concrete blocks (1300 mm

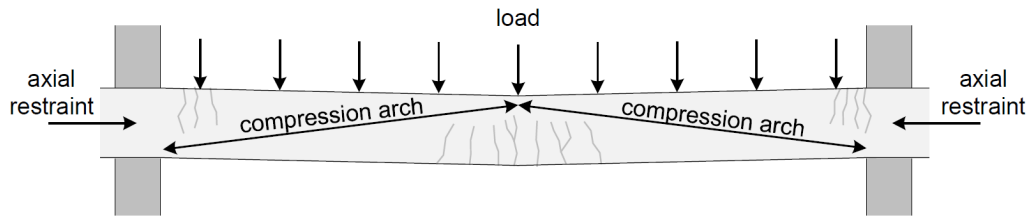


FIGURE 1. Basic principle of compressive membrane action.

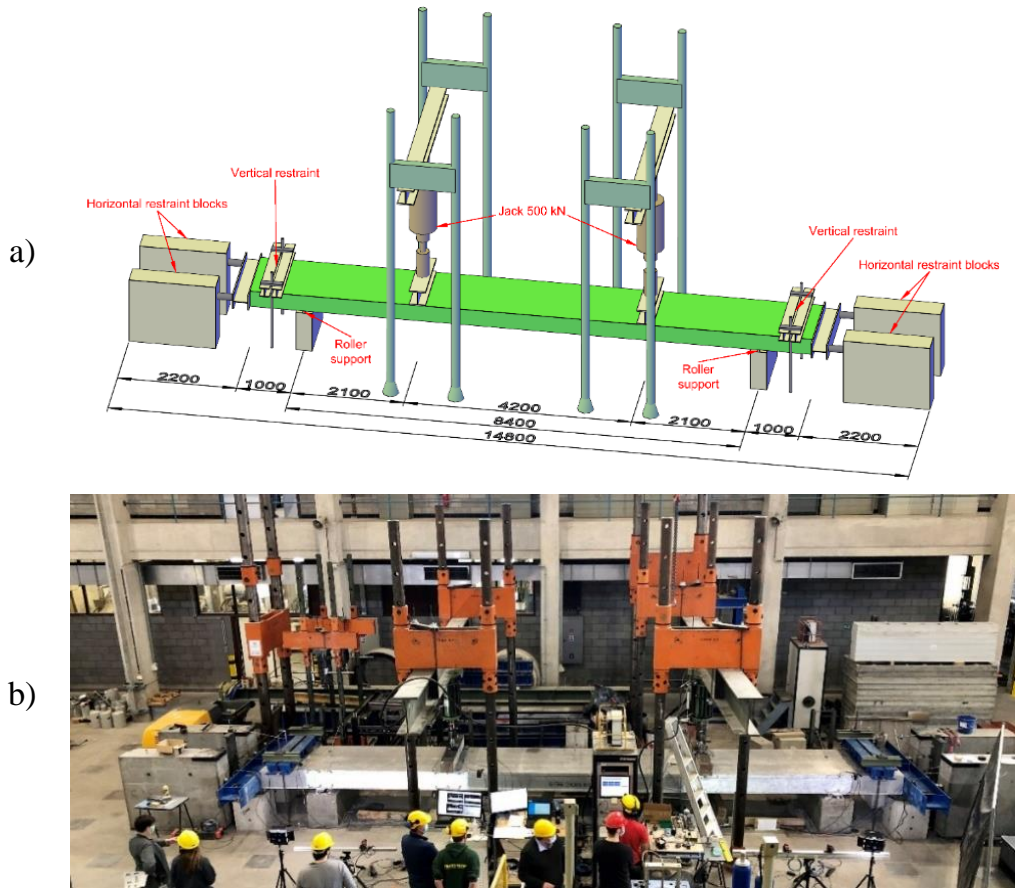


FIGURE 2. Restrained four-point bending test: (a) Schematic overview (dimensions in mm); (b) picture of the actual test set-up [6].

× 400 mm × 1600 mm) that were anchored in the laboratory strong floor. Additionally, uplifting of the slab ends was prevented by two steel profiles, which were anchored to the lab floor with high-grade steel rods. This particular setup allowed for the formation of significant compressive membrane forces inside a real-size HC slab. In the unrestrained test, these end restraints were removed, and the outward expansion and rotation of the slab was not hindered.

2.1. TEST RESULTS

During the tests, the vertical and horizontal displacements were measured using 9 displacement transducers. The applied forces and horizontal forces on the restraint blocks were also continuously measured using 6 load cells. In the two restrained tests, the slabs reached a capacity of respectively 298 kN and 269 kN per load application point, which was significantly

higher than the unrestrained setup (capacity = 180 kN). The maximum horizontal reaction force measured in the restrained tests was 1221 kN and 779 kN for HC1 and HC2 respectively. In both tests, the horizontal restraint stiffness of approximately 250 kN/mm was observed. This values was derived from the measurements of the restraint forces and horizontal displacement of the slab ends.

The load displacement graphs from the three tests are depicted in Figure 4a. Both restrained slabs collapsed after a brittle web shear failure, whereas the unrestrained slab exhibited a more ductile behaviour. Even though the test setup was identical in test HC1 and HC2 a significant difference in the ultimate capacity and deflection at failure was observed. For further details on the experimental campaign the reader is referred to [6].

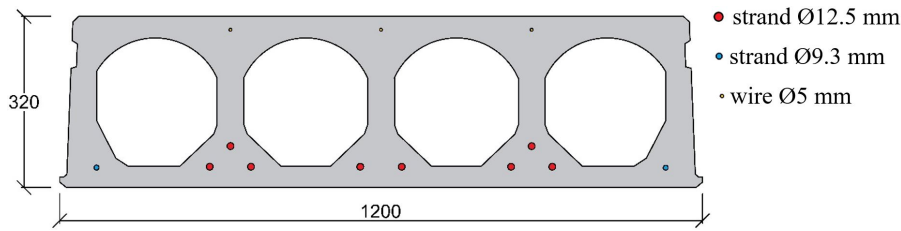


FIGURE 3. Hollow core slab section (dimensions in mm).

Test	Age (days)	$f_{c,cube}$ (MPa)	$f_{c,cyl}$ (MPa)	f_{ct} (MPa)
HC1	68	75.7	64.3	3.85
HC2	71	74.9	65.6	3.63
HC3	85	78.1	68.1	3.63

TABLE 1. Sample characteristics of material properties for concrete.

Strand/wire	$f_{p0.2}$ (MPa)	f_m (MPa)	ε_u (%)	E_p (GPa)
HC1	1789	1975	6.25	221.5
HC2	1782	1938	5.21	218.1
HC3	1627	1848	5.94	193.9

TABLE 2. Sample characteristics of material properties for prestressing steel.

2.2. MATERIAL TESTS

The tested HC slabs were made of C50/60 concrete. To obtain the actual mechanical properties of the concrete, compressive tests on cube samples (150 mm \times 150 mm \times 150 mm), cylinder samples (diameter 150 mm, height 300 mm) and flexural bending tests on prism samples (400 mm \times 100 mm \times 100 mm) were performed, see Table 1. The prestressing strands (bottom reinforcement) have a specified characteristic tensile strength of 1860 MPa. The prestressing wires (top reinforcement) have a specified characteristic tensile strength of 1770 MPa. To obtain the actual mechanical properties, tensile tests were performed on the three types of prestressing reinforcement. From the obtained stress-strain curves, the values for the 0.2% strain limit $f_{p0.2}$, tensile strength f_m , ultimate strain ε_u and Young's modulus E_p were derived, see Table 2. These values were used as inputs for the material models in the numerical models.

3. FINITE ELEMENT MODELLING

3.1. MODEL VALIDATION

In parallel with the experimental tests, a detailed 3D numerical model was developed using the finite element (FE) software Abaqus [7]. Herein, nonlinear material models were employed to model the behaviour of the concrete and prestressing steel under large deformations in an adequate manner. The concrete was modelled using the Abaqus concrete damaged plasticity model. Herein, the stress-strain diagrams for concrete in compression and tension were based on EN 1992-1-2 [8] and fib Model Code 2010 [9], respectively. The prestressing steel was modelled using a bilinear

stress-strain diagram. For each model evaluation, the material properties in accordance with Table 1 and 2 were used.

In the numerical evaluations, 8-noded hexahedral (brick) elements (C3D8) and 2-noded linear truss elements (T3D2) are used to model the concrete and steel prestressing strands, respectively. Assuming perfect bond, the prestressing strands are embedded within the concrete element, using the embedded constraint option in Abaqus. The supports and end restraints were modelled to precisely correspond to the test setup.

Overall, the model is able to predict the experimentally obtained load-displacement curves, the failure mode and crack patterns with high accuracy, as shown in Figure 4a and Figure 4b, respectively. Only for the case of HC1, the model somewhat underestimates the deflection and load at failure.

3.2. INFLUENCE OF CONCRETE TENSILE STRENGTH

As observed in the experimental tests, the ultimate capacity $F_{Q,max}$ and horizontal restraint force $F_{H,max}$ of the HC slabs in the restrained setup exhibit a large variability. Even though the test setup was identical for HC1 and HC2, the difference in the measured ultimate capacity was close to 30 kN. Furthermore, the difference in the maximum horizontal restraint force was nearly 450 kN. These large differences could be attributed to the brittle shear tension failure mechanism, which was observed in both tests. As shown in Figure 4b, this failure mode is characterized by a diagonal crack, which forms at mid-depth and propagates towards the support and the compression zone,

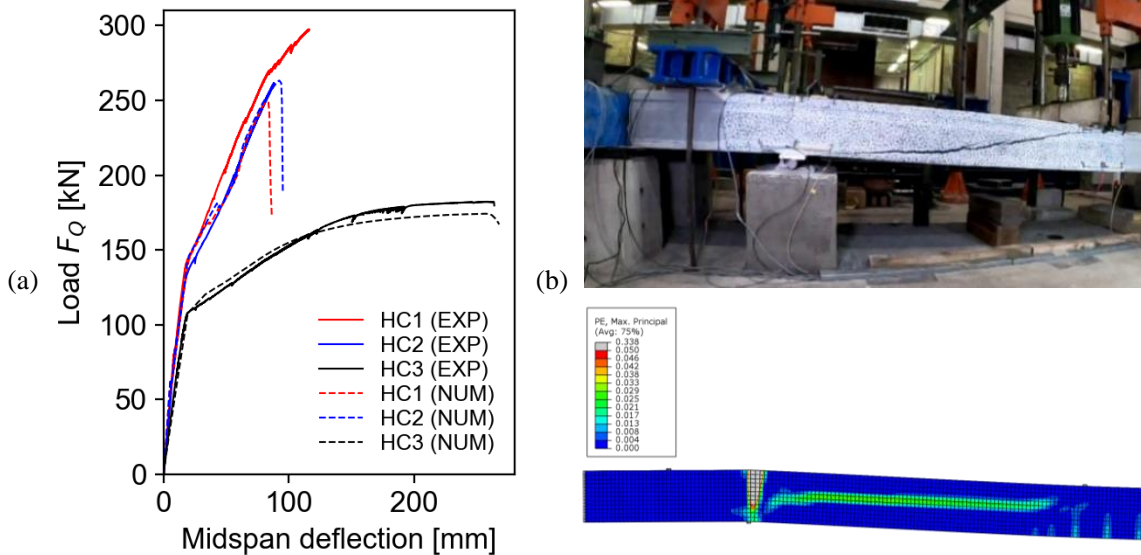


FIGURE 4. Comparison of experimental results and numerical model: (a) load-displacement graphs; (b) crack pattern at failure in restrained test HC1 [6].

thus causing a brittle failure [10]. In the absence of transverse reinforcement in thin-walled webs of the HC slab, the shear capacity of slabs depends only on the tensile strength of the concrete [11]. Hence the concrete tensile strength might considerably influence the capacity of these slabs.

To test this hypothesis, the numerical model for HC1 was re-evaluated for a range of input value for the concrete tensile strength between 3.5 MPa and 5 MPa, as shown in Figure 5. From the obtained load-displacement curves, it is clear that the tensile strength of concrete has a very large influence on the CMA capacity of the HC in the studied test-setup, especially, in the range between 3.5 MPa and 4.5 MPa. The above result highlights the importance of considering the stochastic nature of the concrete tensile strength in a probabilistic assessment of concrete slabs prone to shear failure.

4. PROBABILISTIC MODEL

In the following section, a stochastic evaluation of the previously presented FE model is performed, in order to obtain the distributions of the ultimate capacity $F_{Q,max}$ of prestressed HC slabs in restrained and unrestrained conditions. In the restrained configuration also the distribution of the maximum membrane force $F_{R,max}$ (i.e. the horizontal force in the slab) is evaluated. Given the significant computational power required for a single FE model evaluation, it would be impractical to perform such an analysis by evaluating a set of traditional Monte Carlo simulations. Hence, a Latin Hypercube Sampling scheme was used to keep the number of model evaluations to a minimum. Furthermore, four key variables were selected, which are considered as the most influencing with respect to the determination of the ultimate load capacity, especially in case of the occurrence of CMA. The key

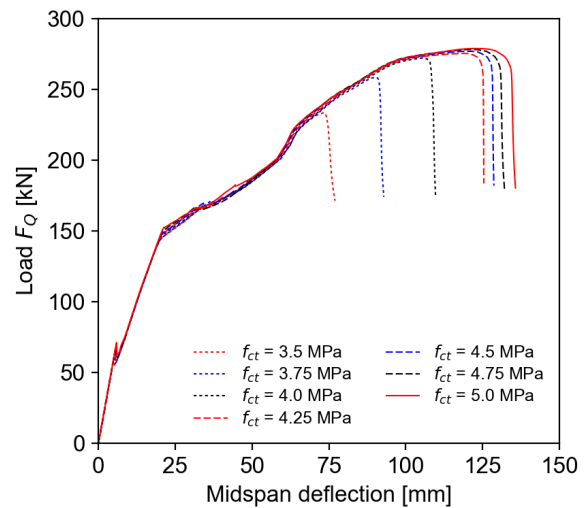


FIGURE 5. Influence of the concrete tensile strength f_{ct} on the load-displacement behaviour of restrained hollow core slabs.

variables are the concrete compressive strength f_c , the concrete tensile strength f_{ct} , the initial prestress σ_{pi} and the spring constant k corresponding to the horizontal restraints.

The probabilistic models for concrete material properties and the initial prestress of the steel reinforcement are based on [12, 13], as presented in Table 3. Herein, the mean values for the concrete compressive and tensile strength are based the values of HC1, in accordance with Table 1. As a first approximation, the concrete compressive strength and tensile strength have been considered independent. To study the influence of the axial restraint stiffness, two values for the spring constant k are considered, i.e. 50 kN/mm and 250 kN/mm. The latter value corresponds to

Property	Distr.	μ	COV
Concrete compressive strength f_c	LN	64.3 MPa	0.06
Concrete tensile strength f_{ct}	LN	3.85 MPa	0.3
Initial prestress σ_{pi}	N	1116 MPa	0.06
Spring constant k of horizontal restraints	LN	case dependent (kN/mm)	0.25

TABLE 3. Probabilistic models for most important basic variables involved in the uncertainty quantification of the compressive membrane action in the investigated hollow core slabs.

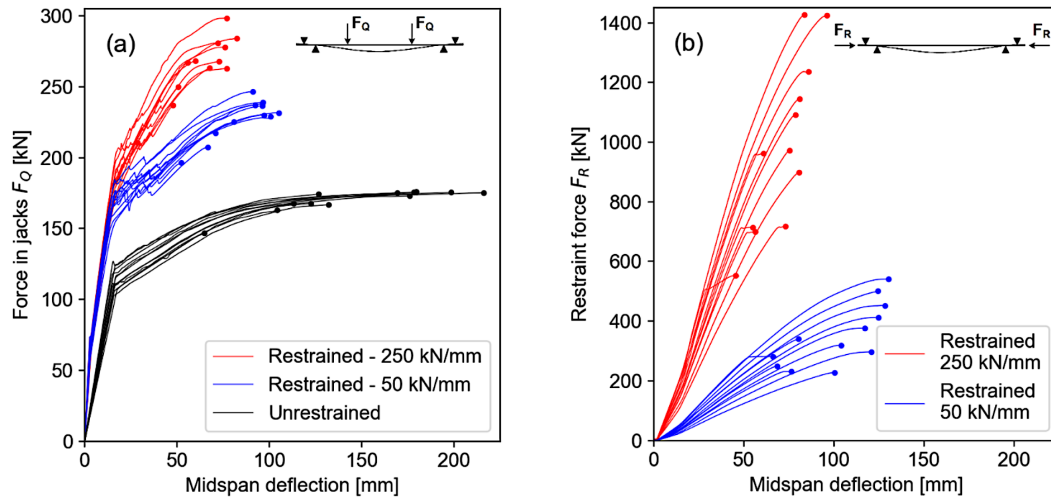


FIGURE 6. LHS samples of restrained and unrestrained hollow core slabs; (a) the load-displacement curves (b) restraint force versus displacement curves.

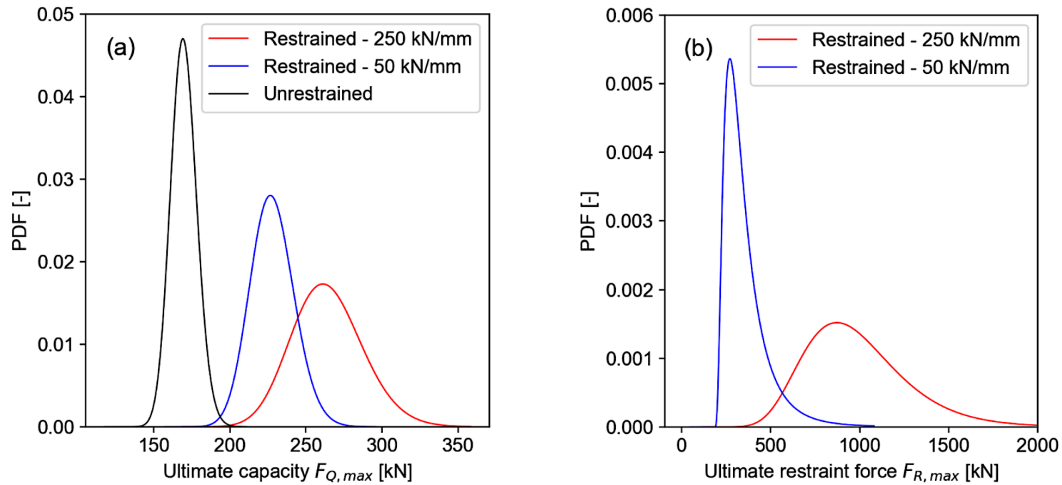


FIGURE 7. (a) PDF of the ultimate capacity $F_{Q,max}$; (b) PDF of the ultimate restraint force $F_{R,max}$.

the stiffness of the restraints in the experiments. The value of 50 kN/mm was chosen to study the influence of a structure with a lower restraint stiffness on the development of CMA in precast hollow core slabs. The probabilistic model for the spring stiffness is based on [14].

5. RESULTS

In total, three stochastic FE analyses were performed: two restrained cases and one unrestrained case. For each case, a set of 12 Latin Hypercube Samples of

the input variables were generated according to the method described in [15]. Figure 6a depicts the numerically obtained load-displacement curves from the FE evaluations, for the unrestrained case and two restraint stiffnesses. The curves are displayed up to the point of failure (i.e. bending or shear tension failure). From the graph, it is clear that a higher restraint stiffness corresponds to a higher ultimate capacity $F_{Q,max}$ and a reduced deflection at failure.

The curves in Figure 6b show the horizontal restraint force F_R as a function of the midspan deflec-

Calculation	Distribution	μ	COV
Restrained - 250 kN/mm	LN	264.1 kN	0.084
Restrained - 50 kN/mm	LN	227.1 kN	0.062
Unrestrained	LN	169.8 kN	0.048

TABLE 4. Probabilistic models for the ultimate load-carrying capacity $F_{Q,max}$.

Calculation	Distribution	μ	COV
Restrained - 250 kN/mm	LN	986.7 kN	0.279
Restrained - 50 kN/mm	LN	352.5 kN	0.286

TABLE 5. Probabilistic models for the maximum horizontal restraint force $F_{R,max}$.

tion. In these curves, the restraint force increases monotonically, up to the point at which the ultimate capacity $F_{Q,max}$ is reached. Thereafter the restraint forces reduce rapidly (not shown in the graph). The graph illustrates that a higher restraint stiffness corresponds to a higher maximum restraint force $F_{R,max}$.

Figure 7a shows the distribution of the ultimate load-carrying capacity $F_{Q,max}$, for each of the three considered cases, assuming a lognormal distribution. From this graph, it is clear that the variability of $F_{Q,max}$ increases significantly with an increased restraint stiffness. Additionally, Figure 7b depicts the distribution of the maximum restraint force $F_{R,max}$. This graph clearly illustrates the presence of a very large variability in the ultimate restraint force.

Considering the LHS samples in combination with the FE analyses, probabilistic models for the load-carrying capacity and maximum restraint force of both the restrained and unrestrained cases are presented in Table 4 and Table 5 respectively. A lognormal distribution is assumed for both variables. The results in Table 4 show that the coefficient of variation (COV) of the ultimate capacity $F_{Q,max}$ is higher for the restrained cases, and increases with increasing axial restraint stiffness. Table 5 on the other hand, indicates no significant difference in the value of the COV of the maximum horizontal restraint force $F_{R,max}$ for both restraint cases.

6. CONCLUSIONS

In the present paper, a stochastic finite element analysis was performed to study the influence of stiff lateral restraints on the load-displacement behaviour of precast concrete hollow core slabs. The finite element model was validated against a set of real-scale experimental tests, and was applied in combination with probabilistic models for the most influencing variables to execute Latin Hypercube Simulations of the load-carrying capacity. Based on the random simulations, probabilistic models for the load carrying capacity and horizontal restraint force are established.

In general, it can be concluded that the presence of lateral restraints strongly influences the variability of the ultimate load-carrying capacity. The coefficient

of variation (COV) of the ultimate capacity increases from 0.048 in the unrestrained case to 0.084 for the highly restrained case with an axial restraint stiffness of 250 kN/mm. Furthermore, a high COV of the horizontal restraint force was observed. This value was observed not to change significantly with respect to the two stiffnesses of the surrounding structure considered.

ACKNOWLEDGEMENTS

This research has been made possible through funding from the Research Foundation Flanders (FWO), which is gratefully acknowledged (Grant number 11F5520N).

REFERENCES

- [1] L. K. Guice, E. J. Rhomberg. Membrane Action in Partially Restrained Slabs. *ACI Structural Journal* **85**(4), 1988. <https://doi.org/10.14359/2517>.
- [2] G. I. B. Rankin, A. E. Long. Arching Action Strength Enhancement in Later Ally-Restrained Slab Strips. *Proceedings of the Institution of Civil Engineers - Structures and Buildings* **122**(4):461-7, 1997. <https://doi.org/10.1680/istbu.1997.29834>.
- [3] K. Thoma, F. Malisia. Compressive membrane action in RC one-way slabs. *Engineering Structures* **171**:395-404, 2018. <https://doi.org/10.1016/j.engstruct.2018.05.051>.
- [4] F. J. Vecchio, K. Tang. Membrane action in reinforced concrete slabs. *Canadian Journal of Civil Engineering*, **17**:686-697, 1990. <https://doi.org/10.1139/190-082>.
- [5] K. S. Elliott, C. K. Jolly. *Multi-storey Precast Concrete Framed Structures*. John Wiley & Sons, Oxford UK, 2013.
- [6] T. Thienpont, W. De Corte, R. Van Coile, et al. Compressive membrane action in axially restrained hollow core slabs: Experimental investigation. *Structural Concrete*, 2022. <https://doi.org/10.1002/suco.202100684>.
- [7] Dassault Systemes. *Abaqus 6.14: Abaqus/CAE User's Guide*. Providence, USA, 2014.
- [8] CEN. EN 1992-1-2. *Eurocode 2 - design of concrete structures. Part 1-2: general rules - structural fire design*. Brussels. <https://www.phd.eng.br/wp-content/uploads/2015/12/en.1992.1.1.2004.pdf>.

- [9] Fib. fib Model Code 2010, Final draft - Volume 1. Comité Euro-International Du Béton, 2010. <http://repositorio.unan.edu.ni/2986/1/5624.pdf>.
- [10] C. A. M. Araujo, D. D. Loriggio, J. M. M. N. Da Camara. Anchorage failure and shear design of hollow-core slabs. *Structural Concrete* **12**(2):109-19, 2011. <https://doi.org/10.1002/suco.201000024>.
- [11] W. Derkowski, M. Surma. Prestressed hollow core slabs for topped slim floors - Theory and research of the shear capacity. *Engineering Structures* **241**, 2021. <https://doi.org/10.1016/j.engstruct.2021.112464>.
- [12] JCSS. *Probabilistic Model Code - Part 3.1: Concrete properties*. In The Joint Committee on Structural Safety, 2000.
- [13] JCSS. *Probabilistic Model Code - Part 3.4: Static properties of prestressing steel*. In The Joint Committee on Structural Safety, 2000.
- [14] R. Caspeepe, D. Gouverneur, R. Van Coile, et al. Structural reliability of concrete slabs considering tensile membrane action. In *Safety, Reliability and Risk Analysis*, p. 2713-20, 2013. <https://doi.org/10.1201/b15938-410>.
- [15] A. Olsson, G. Sandberg, O. Dahlblom. On Latin hypercube sampling for structural reliability analysis. *Structural Safety* **25**(1):47-68, 2003. [https://doi.org/10.1016/s0167-4730\(02\)00039-5](https://doi.org/10.1016/s0167-4730(02)00039-5).